Unconventional Sources of Error in High-Resolution Wide-Swath SAR Systems based on Scan-On-Receive

Federica Bordoni [a], David Lind [a,b], Andreas Jakobsson [b], Gerhard Krieger [a]
[a] Microwaves and Radar Institute, German Aerospace Centre (DLR), Germany
[b] Centre for Mathematical Sciences, Mathematical Statistics, Lund University, Sweden

Abstract

The scan-on-receive (SCORE) is a key digital beamforming (DBF) technique for future high-resolution wide-swath synthetic aperture radar (SAR) systems. A sharp and high gain receive beam, steered in real time towards the expected direction of arrival (DoA) of the backscattering signal, allows for improved SAR imaging performance with respect to a conventional approach. Nevertheless, it also exposes the system to new errors, associated with a mismatch between the expected and the actual DoA. This paper identifies possible sources of error, specific of SCORE-based systems, and investigates their effect on the SAR image quality in dependence of instrument and geometrical parameters.

1 Introduction

The scan-on-receive (SCORE) [1] is one of the most relevant digital beamforming (DBF) techniques for high-resolution wide-swath synthetic aperture radar (SAR) systems [3]-[7]. It is considered for advanced missions, such as the United States-Indian NISAR, the European Sentinel-1 Next Generation, and the German Tandem-L [5]-[7].

According to SCORE, a large swath is illuminated by using a wide transmit (Tx) beam; whereas on receive (Rx), multiple digital channels are used to realize a sharp and high gain beam, that scans the illuminated swath from near to far range, following the pulse echo as it travels along the ground range direction [1]. The mentioned, original SCORE technique was then extended by more complex concepts, involving the use of multiple Rx beams or incorporating null-steering techniques, to further enhance the achievable SAR image quality [3], [4].

With respect to a conventional approach, SCORE allows for improved radiometric performance all over the swath, as well as a more efficient suppression of range ambiguous signals. Nevertheless, a full exploitation of the advantages offered by SCORE-based systems is constrained by the knowledge of the direction of arrival (DoA) of the Rx signals, useful and ambiguous. This is a prerequisite to properly collect the backscattered energy of interest, and to effectively suppress undesired returns. Accordingly, SCORE-based systems could be sensitive to unconventional errors, associated with a mismatch between the expected and the actual DoA of the Rx signal. A specific error and performance analysis is of interest, which accounts for effects that for conventional systems may be negligible, such as radiometric variations induced by pulse duration [8] and terrain morphology [9].

A first attempt to thoroughly describe these unconventional errors, and characterize their relevance in relation to instrument and acquisition geometry parameters, was recently published in [10]. This paper recalls and extends that study, by investigating how these errors affect the SAR image quality.

2 Steering Errors

Main sources of unconventional errors, associated with a mismatch between the expected and the actual DoA of the Rx signal, include: topographic variations, pulse duration, range cell migration (RCM), and pulse bandwidth [10]. The amount of error depends on the instrument parameters and the acquisition geometry. In particular, for a given unmodelled terrain elevation, the steering error changes according to the orbit height and the range position. The error associated with the pulse duration depends on the acquisition geometry too, and additionally on the SCORE steering velocity. The RCM steering error, on the radar wavelength and the azimuth resolution. The pulse bandwidth introduces an error according to the pattern behaviour versus frequency [10].

As an example, Fig. 1 and 2 describe, respectively, the angular mismatch induced by an unmodelled terrain height and pulse duration, in relation to the acquisition geometry. Both figures evidence larger errors in near range, and for lower orbit heights: around 23 deg incidence angle, for an orbit height of 500 km, the errors could reach values of about 0.5 deg and 1 deg, respectively. For range ambiguities, located in near range, the errors are even larger.

3 Image Quality Degradation

The effect of steering errors on the radiometric properties of the image is here investigated, both from a numerical and theoretical perspective. The focus is on errors generated by an unmodelled terrain height and pulse duration.

The frequency dispersion of the SCORE Rx pattern over the chirp band is neglected, as well as the RCM.

For simplicity, a planar array antenna and a stripmap operational mode are considered. More in detail, an antenna with K digital Rx elevation channels, uniformly distributed along the height, in such a way that the SCORE Rx pattern can be approximated with its array factor (AF).

Based on the previous assumptions, SCORE behaviour can be investigated by considering only the processing in the range dimension [9]. Specifically, the following simulation frame is considered. The imaged scene is modelled as a set of N_a discrete sequences of scatterers (range lines). Each of the N_a sequences is associated with a given azimuth instant. Within a single discrete sequence, the scatterers are positioned along the range direction, and spaced by the range sampling interval, assumed to be (approximatively) equal to the range resolution cell size. The signal backscattered

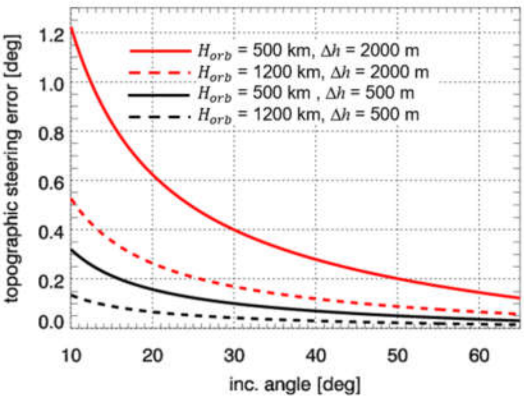

Figure 1 Steering error due to unmodelled terrain elevation, Δh, versus incidence angle, for different orbit heights, H_{orb}. SCORE steering is computed assuming no terrain elevation.

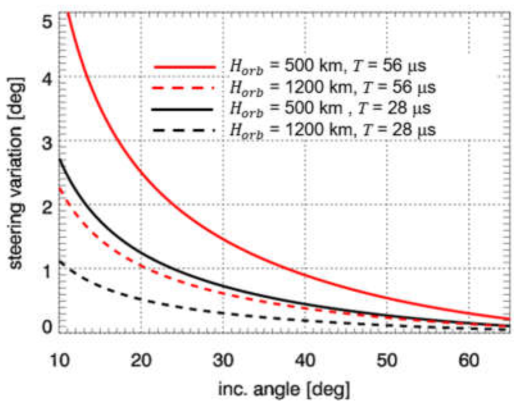

Figure 2 SCORE steering variation during a time interval equal to the pulse duration, T, versus incidence angle, for different orbit heights, H_{orb}, and T values. SCORE steering computed based on the centre of the pulse and no terrain height. The maximum steering error associated with T is about half the steering variation.

by each discrete sequence is then described by the reflectivity function. For instance, the reflectivity is a Dirac delta, for a point target; while, for a distributed uniform target, it is a white complex Gaussian (WCG) process, where each sample is CG distributed, with zero mean and variance (mean power), σ^2, given by the "radar cross section" of the resolution cell [11].

As regards the image formation process, for a conventional (single channel) system, the Rx signal is obtained by the convolution of the Tx chirp with the reflectivity, and the SAR processing reduces to the range compression. For a SCORE-based system, the reflectivity, "seen" by each elevation channel, includes the interferometric phase term, according to the actual DoA, $\bar{\theta}_{act}$. SCORE pattern steering is then performed on the set of K raw data, by including a range-time dependent phase term, based on the expected DoA, $\bar{\theta}_{\exp}$, and adding up the K signals. Finally, the range compression is applied [9]. All the signals are in baseband.

To describe SCORE effect on the radiometric quality of the image, the SCORE loss (SL) is here defined as:

$$SL(t) = \frac{P_s(t)}{K^2\, P_c(t)} \tag{1}$$

where, P_s is the power of a pixel obtained by SCORE; P_c the power of the same pixel obtained by conventionally processing a single channel; t, the pixel range position (in two-way time delay).

The SL is evaluated numerically by simulating the imaging process. Note, that in case of a point target, the power in eq. (1) is the (deterministic) intensity of the pixel, i.e. the peak power of the impulse response; whereas for a resolution cell of a uniform target, it is the mean intensity of the pixel, i.e. the pixel intensity averaged over the azimuth dimension.

A novel theoretical expression for the SL in eq. (1) is derived, for a point target and a uniform target, respectively:

$$SL_p(t_0) \cong \left| \sum_{t=t_0-T/2}^{t_0+T/2} AF_n\left(\bar{\theta}_{\exp}(t), \bar{\theta}_{act}(t_0)\right) \right|^2 \Big/ N_s^2 , \tag{2}$$

$$SL_u(t_0) \cong \sum_{t=t_0-T/2}^{t_0+T/2} \left| AF_n\left(\bar{\theta}_{\exp}(t), \bar{\theta}_{act}(t_0)\right) \right|^2 \Big/ N_s , \tag{3}$$

where, T denotes the pulse duration, and N_s the corresponding number of samples; t the (discretized) two-way time delay; t_0 the two-way time delay at the target/resolution cell; $\bar{\theta}_{\exp}(t)$ the expected DoA; $\bar{\theta}_{act}(t_0)$ the actual DoA associated with the position of the target/resolution cell; AF_n the normalized SCORE array factor, steered towards $\bar{\theta}_{\exp}(t)$ and computed in $\bar{\theta}_{act}(t_0)$.

Both the previous theoretical expressions reflect the fact that each sample, received from a given DoA, $\bar{\theta}_{act}(t_0)$, during the pulse duration, is weighted by different SCORE pattern values, according to the SCORE steering law,

$\overline{\theta}_{\exp}(t)$. Nevertheless, in case of a point target, the samples add coherently in voltage; whereas, they add in power for the uniform target.

Eq. (2) and (3) state that the SL is negligible, if two conditions are simultaneously satisfied: (i) $\overline{\theta}_{\exp}(t_0) \approx \overline{\theta}_{act}(t_0)$; (ii) SCORE steering angle variation within the pulse duration is small w.r.t. SCORE half power beam-width. Otherwise, a loss occurs. This loss is different for a point and a uniform target, depends on SCORE pattern shape and steering velocity, on the topography, the pulse duration, and the location of the target (in near or far range).

It is worth noting that the derived theoretical expressions are valid also for a range ambiguous target/resolution cell, and for an arbitrary SCORE steering law, $\overline{\theta}_{\exp}(t)$.

The SL is further investigated numerically, as shown in Fig. 3 and 4. In particular, for a distributed uniform target, N_a = 1000 realizations of a WCG process are generated as reflectivity. These are then used to simulate the SCORE SAR image and to evaluate, according to eq. (1), the SL. The theoretical SL, given by eq. (2) and (3), are computed too. Additionally, the case of a very short pulse is considered for comparison. SCORE beam is steered towards the centre of the pulse, assuming no terrain elevation.

Two different scenarios are investigated: in one, the unmodelled terrain elevation, Δh, changes versus range; in the other, Δh is constant and the backscattered signal is received in proximity of a pattern null. The second scenario could represent the case of a received ambiguous signal. In both cases, $T \neq 0$.

In Fig. 3, the considered Δh is 0 m in near range, then it increases linearly until 2000 m, and remains constant in far range; T = 56 μs. In Fig. 4, Δh is constant and T = 28 μs. As regards the other parameters: H_{orb} = 514 km; the antenna height, h_{ant} = 1 m; the radar wavelength, λ = 3.1 cm.

The results obtained for the distributed uniform (WCG) target confirm the agreement between the theoretical SL_u and the simulated SL. The simulated SL evidences additionally a possible radiometric instability, related to the pattern values weighting the Rx signal. A comparison between the loss for a point target, SL_p, and that for a uniform target shows that the difference between the two losses can be huge in correspondence of pattern nulls (Fig. 4). The strong influence of the pulse length on the loss is highlighted by the SL for a very short pulse: here the loss is determined only by the value of the SCORE pattern weighting the pulse centre.

These first results, even if limited, suggest that the unconventional errors, associated with topography and pulse duration, cannot be neglected, especially considering the demanding requirements on the radiometric quality imposed on SAR images (the required accuracy and stability are in the order of 0.5 dB). The dependence on the imaged scene deserves attention too.

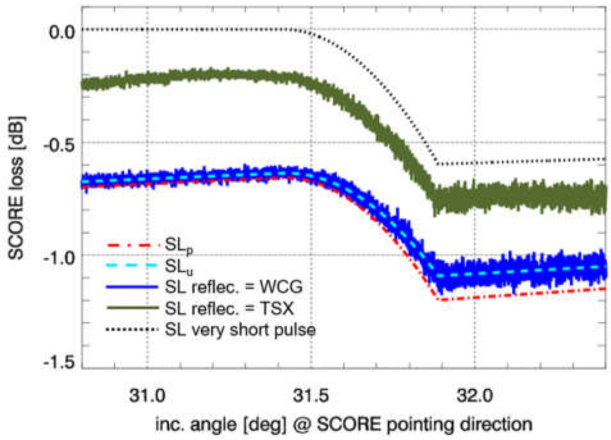

Figure 3 SL_p in eq. (2), SL_u in eq. (3), SL in eq. (1). SL computed for: a WCG reflectivity (N_a = 1000 realizations); a reflectivity from a homogeneous TSX image (N_a = 1000 lines); a very short pulse. The samples of the WCG reflectivity and the TSX image have the same mean and variance. Δh: 0 m in near range; linearly increasing from 0 m to 2000 m in mid range; 2000 m in far range. T = 56 μs; H_{orb} = 514 km; h_{ant} =1 m; λ=3.1 cm; K=24.

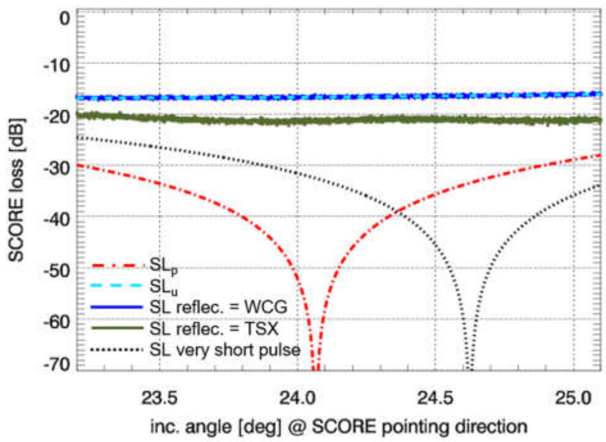

Figure 4 SL_p in eq. (2), SL_u in eq. (3), SL in eq. (1). SL computed for: a WCG reflectivity (N_a = 1000 realizations); a reflectivity from a homogeneous TSX image (N_a = 1000 lines); a very short pulse. The samples of the WCG reflectivity and the TSX image have the same mean and variance. Δh=7500 m (actual DoA around a pattern null). T = 28 μs; H_{orb} = 514 km; h_{ant} =1 m; λ=3.1 cm; K=24.

It is worth to remark that eq. (3) is derived assuming that the reflectivity samples, i.e. the signal backscattered from different resolution cells, are uncorrelated. If a correlation is present, the SL changes. This could be understood by considering the expression of a single sample of the Rx SAR raw data signal, after SCORE is applied:

$$s(t_0) = \sum_{t=t_0-T/2}^{t_0+T/2} r(t)\, c(t_0 - t)\, AF_n\left(\bar{\theta}_{\exp}(t_0), \bar{\theta}_{act}(t)\right), \quad (4)$$

where (a scaling factor is neglected), $r(t)$ denotes the reflectivity, $c(t)$ the Tx chirp pulse, AF_n the normalized array factor steered towards $\bar{\theta}_{\exp}(t_0)$ and computed in $\bar{\theta}_{act}(t)$, i.e. the summation is done over the instantaneous ground range extension of the chirp. For the ideal uniform target, the integrated reflectivity samples, $r(t)$, are uncorrelated random variables, distributed as CG(0, σ^2), and the mean power of the signal in eq. (4) is:

$$E\left\{\left|s(t_0)\right|^2\right\} = \sigma^2 \sum_{t=t_0-T/2}^{t_0+T/2} \left|AF_n\left(\bar{\theta}_{\exp}(t_0), \bar{\theta}_{act}(t)\right)\right|^2. \quad (5)$$

Nevertheless, if the integrated reflectivity samples are correlated, then cross terms affect the expected value, and the mean power cannot be simplified to the expression in (5).
The effect of a possible correlation on the SL is shown in Fig. 3 and 4, by the green curve. Here, the reflectivity function, used to simulate the SL, is obtained from a homogeneous real TerraSAR-X (TSX) image (single look, slant range, complex), acquired over the Amazonas forest. Specifically, a single realization of the reflectivity is given by a range line of the TSX image.
Due to the SAR processing, the pixels of the TSX SAR image are correlated. As expected, the obtained SL deviates from the SL of the ideal, WCG, uniform target, even if all the other simulation parameters (included mean and variance of the reflectivity samples) are equal. In particular, Fig. 3 and 4 show that the difference could be significant, depending also on the pattern values weighting the Rx signal. This highlights the relevance of a proper simulation of the reflectivity.

4 Conclusions

With respect to conventional SAR systems, SCORE-based systems are exposed to new errors, associated with a mismatch between the expected and the actual DoA. The main sources of error include topographic variations and pulse duration. The paper investigates their effect on the SAR image quality analytically and numerically. The first results show that both the radiometric and range ambiguity performance could degrade in a relevant way. The dependence on the imaged scene deserves attention too. In fact, the amount of degradation differs in case of point and distributed targets, and depends, for a given pulse length and unmodelled terrain height, on the SCORE pattern shape and steering velocity, the target location within the image, and the statistical properties of the backscattering.

References

[1] M. Suess, B. Grafmueller, R. Zahn, “A Novel High Resolution, Wide Swath SAR System”, in Pro. IGARSS, vol. 3, pp. 1013-1015, July 2001.

[2] N. Gebert, G. Krieger, and A. Moreira, "Digital Beamforming on Receive: Techniques and Optimization Strategies for High-Resolution Wide-Swath SAR Imaging", IEEE Tran. on Aero. and Electron. Sys., vol. 45, no. 2, pp. 564-592, April 2009.

[3] G. Krieger, N. Gebert, A. Moreira, "Multidimensional Waveform Encoding: A New Digital Beamforming Technique for Synthetic Aperture Radar Remote Sensing", IEEE Tran. on Geosci. and Remote Sen., vol. 46, no. 1, pp.31-46, Jan. 2008.

[4] F. Feng, S. Li, W. Yu, P. Huang, W. Xu, "Echo Separation in Multidimensional Waveform Encoding SAR Remote Sensing Using an Advanced Null-Steering Beamformer", IEEE Tran. on Geosci. and Remote Sen., vol. 50, no. 10, pp.4157-4172, Oct. 2012.

[5] S. Huber, M. Villano, M. Younis, G. Krieger, A. Moreira, B. Grafmueller, R. Wolters, “Tandem-L: Design Concepts for a Next-Generation Spaceborne SAR System”, Pro. EUSAR, June 2016.

[6] P. Rosen, S. Hensley, S. Shaffer, W. Edelstein; Y. Kim; R. Kumar; T. Misra; R. Bhan; R. Satish; R. Sagi, “An update on the NASA-ISRO dual-frequency DBF SAR (NISAR) mission”, Pro. IGARSS, July 2016.

[7] Adamiuk, C. Schaefer, C. Fischer, and C. Heer, “SAR Architectures Based on DBF for C- and X-Band Applications”, Pro. EUSAR, June 2014.

[8] M. Younis, T. Rommel, F. Bordoni, G. Krieger, A. Moreira, “On the Pulse Extension Loss in Digital Beamforming SAR”, IEEE Geosci. and Remote Sen. Letters, Vol. 12, No. 7, pp. 1436 – 1440, Oct. 2015.

[9] F. Bordoni, M. Rodriguez, P. Prats, G. Krieger, “The Effect of Topography on SCORE: an Investigation Based on Simulated Spaceborne Multichannel SAR Data”, Pro. EUSAR, pp.1130-4, June 2018.

[10] F. Bordoni, M. Rodriguez, G. Krieger, “Possible Sources of Imaging Performance Degradation in Advanced Spaceborne SAR Systems Based on Scan-On-Receive”, Proc. RadarConf, Sept. 2020.

[11] A. Freeman, C. Curlander, “radiometric correction and calibration of SAR images”, Photogrammetric Engineering & Remote Sensing, 1989.